RT E JOURNAL

Surface treatment of additively manufactured high-alloy austenitic steel parts with the aim of prolonging the fatigue life

Dr. Kristina Navickaitė [a,b], Stefan Langenhan (M.Sc.) [c], Anastasiia Sherstneva (M.Sc.) [d], Jenny Köckritz (M.Sc.) [a], Dr. rer. nat. Klaus Nestler [b], Michael Penzel (M.Sc.) [e], Dr.-Ing. Anja Weidner [c], Dr.-Ing. Marco Wendler [d], Dr.-Ing. Robert Szlosarek [a], Prof. Dr.-Ing. Horst Biermann [c], Prof. Dr.-Ing. Olena Volkova [d], Prof. Dr.-Ing. Henning Zeidler [a,b], Prof. Dr.-Ing. Matthias Kröger [a]

[a] **Technische Universität Bergakademie Freiberg, Faculty of Mechanical, Process and Energy Engineering, Institute for Machine Elements, Design and Manufacturing**, Agricolastr.1, 09599, Freiberg, Germany

[b] **Beckmann Institute for Technology Development e.V.**, Annabergerstr. 73, 09111, Chemnitz, Germany

[c] **Technische Universität Bergakademie Freiberg, Faculty of Material Science and Technology, Institute of Materials Engineering,** Gustav-Zeuner-Straße 5, 09599, Freiberg, Germany

[d] **Technische Universität Bergakademie Freiberg, Faculty of Material Science and Technology, Institute of Iron and Steel Technology**, Leipziger Straße 34, 09599, Freiberg, Germany

[e] **Plamotion GmbH**, Halsbrücker Str. 34, 09599 Freiberg, Germany

https://doi.org/10.58134/fh-aachen-rte_2024_005

Zusammenfassung In diesem Artikel werden die vorläufigen Ergebnisse einer interdisziplinären Untersuchung an dem hochlegierten austenitischen Stahl mit mittlerem Mangangehalt X2CrMnNi16-7-4,5 vorgestellt. Die Proben wurden mit dem pulverbasierten Elektronenstrahlschmelzverfahren (PBF-EB/M) hergestellt. Das Stahlpulver für das PBF-EB/M-Verfahren wurde mit einer Vakuum-Induktionsschmelz-Gaszerstäubungsanlage (VIGA-1B) gaszerstäubt. Um die Oberflächenintegrität der hergestellten Proben zu verbessern, wurden diese Plasma elektrolytisch poliert (PeP) in Kombination mit Partikelstrahlen, einem vorgelagerten Verfahren. Es wurden für die Endbearbeitung die Verfahren Bad-PeP und Schwall-PeP realisiert.Die Prozessparameter PBF-EB/M wurden ebenfalls optimiert, um die Tiefe der Oberflächenkerben der Proben im eingebauten Zustand zu reduzieren und um Fertigungsfehler, wie z.B. fehlendes Aufschmelzen, zu minimieren.Erste Ergebnisse zeigen, dass das PBF-EB/M-Verfahren für die Bearbeitung von X2CrMnNi16-7-4,5 Stahl gut geeignet ist. Die resultierende Oberflächenqualität erfordert jedoch erhebliche Nachbehandlungsmaßnahmen zur Verbesserung der Oberflächenintegrität. Die Effizienz der angewandten Oberflächenverbesserungstechniken wird anhand der Dicke des abgetragenen Materials, δ, und der Materialabtragsrate *MRR* sowie durch eine qualitative Bewertung des resultierenden Oberflächenzustands bewertet. Es wird gezeigt, dass das Schwall-PeP die effektivste Oberflächenbehandlung für PBF-EB/M-Bauteile ist. Die optimierten Parameter für den Herstellungs- und Nachbehandlungsprozess werden auf die Herstellung eines Tretlagers für ein Lastenfahrrad angewendet, dessen Topologie für eine verlängerte Ermüdungslebensdauer optimiert ist.

Abstract In this article preliminary results of an interdisciplinary study on high-alloy austenitic steel with medium manganese content X2CrMnNi16-7-4.5 are presented. The specimens were manufactured using the powder-based electron beam melting technology (PBF-EB/M). The steel powder for the PBF-EB/M process was gas-atomised using a vacuum induction-melting gas atomisation (VIGA-1B) unit. For improving the surface integrity of the manufactured specimens, they were plasma electrolytic polished (PEP) in a combination with particle blasting. The bath-PEP and standing-wave-PEP processes were realised. The PBF-EB/M process parameters were also optimised in order to reduce the depth of surface notches of the specimens in as-built conditions as well as minimise the building defects, e.g. lack of fusion. The initial results show that while PBF-EB/M process is well suited for processing X2CrMnNi16-7-4.5 steel. The resulting surface quality requires significant post-treatment efforts for improving its integrity. The efficiency of the used surface enhancement techniques is evaluated in terms of the thickness of the removed material, δ, as well as the material removal rate *MRR* and by qualitatively evaluating the resulting surface condition. It is demonstrated that standing-wave-PEP holds the promise for being the most effective surface treatment for PBF-EB/M parts. The optimised parameters for manufacturing and post-treatment processes will be applied for fabricating a bottom bracket of a cargo bike that is topology optimised for prolonged fatigue life.

Introduction

For many decades the research has been focusing on developing material and energy efficient manufacturing processes of goods as well as materials themselves. Thus, additive manufacturing (AM) also known as 3D-printing has evolved and evoked significant interest from academia and industries like medical engineering and energy engineering [1–7]. Various metallic materials have been processed using a vast variety of AM techniques ranging from selective laser melting (PBF-L/M (laser powder bed fusion)), electron beam powder bed fusion (PBF-EB/M), direct energy deposition (DED) [8–11] just to name a few. The most investigated materials are biocompatible titanium alloys [1,12], aluminium alloys [9,13] and few types of stainless steels [14]. More exotic types of materials processed using the AM techniques include bulk metallic glasses, like Vitreloy alloy family and AMZ4 [15,16].

Regarding the development of metallic materials, a major focus is paid to the development of more ductile behaviour and at the same time demonstrating a high yield and tensile strength, less expensive and widely used types of metals, like stainless steel [17,18]. An austenitic high-alloy X2CrMnNi16-7-4.5 steel, reported in [19–24], was proved to meet the requirements above. This high-alloy austenitic steel demonstrates an excellent deformability thanks to transformation induced plasticity and twinning induced plasticity (TRIP/TWIP) [18,19,21,25]. The high formability potential was already demonstrated, that is due to the TRIP/TWIP effect, and cold forming of this materials is more energy efficient [19].

Furthermore, the applicability of high-alloy X2CrMnNi16-7-4.5 steel for PBF-EB/M process was also investigated in [20]. The study concluded, that this alloy system is well suited for layer-based AM processes regardless of the manganese susceptibility to evaporation, which would lead to undesirable instabilities of the phase transformation kinetics [20]. Such instabilities, naturally, could affect mechanical material properties of the final parts.

Another study reported that additively manufactured steel showing TWIP even in as-built condition demonstrates high strength and good ductility [26]. Nevertheless, it is well known that the surface quality, i.e. surface roughness, has a high impact on crack formation and propagation and thus, on the duration of the service life of parts [27–29]. This emphasizes the need of an adequate surface treatment of the parts to meet the specific requirements of different applications.

While there is a large number of various surface treatment methods, not all of them are suitable for additively manufactured parts. Among those methods that could be applied on geometrically complex AM parts are particle blasting (PB), electrochemical polishing (ECP) and plasma electrolytic polishing (PEP). Both ECP and PEP processes bear some similarities, nevertheless their differences are decisive. An extensive comparison of both processes is provided in [30,31], thus it will be omitted in this article. Nevertheless, it is worth to briefly mention the main difference between them, which is the used electrolyte. The ECP process is known to use highly concentrated hazardous acids, while PEP uses weakly concentrated water-based salt solutions, like ammonium sulphate or sodium bicarbonate as electrolytes. It must be noted that the electrolyte used in the PEP process is material specific, i.e. the composition of it is determined by the chemical composition of the material. In this way, a selective material removal could be prevented.

The efficiency of PEP has been already demonstrated on a vast number of different materials ranging from various steels to copper alloys [32–36].

This article reports preliminary results on PBF-EB/M process for manufacturing specimens out of high-alloy austenitic X2CrMnNi16-7-4.5 steel powder produced by the vacuum induction-melting gas atomisation (VIGA-1B) process. The efforts to improve the surface

quality of as-built parts by means of PB and different modes of PEP are discussed as well. The optimal part manufacturing and post treatment parameters will be used in future for producing a bottom bracket of a cargo bike that is topology optimised for a prolonged fatigue life. The currently used method for fatigue optimisation is presented here as well.

Materials and methods

High-alloy austenitic X2CrMnNi16-7-4.5 steel

The austenitic X2CrMnNi16-7-4.5 steel powder for PBF-EB/M process was produced using the VIGA-1B process by atomising powder with various Ni content at TLS Bitterfeld, Germany. Namely 3 wt.%, 6 wt.% and 9 wt.%. These powders were analysed for chemical composition after being re-melted, particle size distribution (PSD), shape, morphology, structure and sphericity. The re-melting was carried out with a middle frequency induction heating furnace *MFG 40* (Linn High Therm GmbH, Germany), the PSD was analysed using a laser diffractometer *LA-960* (Horiba, Japan) the morphology and the structure were analysed using an incident light microscope *Axio Scope.A1* (Zeiss, Germany). The chemical composition of the powder was analysed by means of spark emission spectrometer *Foundry Master UV* (Oxford Instruments). Using *G4 Icarus* and *G8 Galileo* (Bruker AXS GmbH, Germany) combustion analysers the C / S and the N content of the steels were determined, respectively.

For obtaining the powder for PBF-EB/M with the desired chemical composition and structural as well as mechanical properties, initially atomised powder with Ni content of 3 wt. 9 wt. % were mixed with the ratio 4:1. Out of this powder mix the test specimens for analysing the material properties were produced using the *Arcam A2X* (Arcam EBM, Sweden) PBF-EB/M machine. The scanning electron microscopy (SEM) was used to evaluate the powder morphology and surface quality of the as-built specimens. The electron backscatter diffraction method (EBSD) was used to analyse the resulting structure of the as-built PBF-EB/M specimens.

Surface treatment

The initial surface roughness, characteristic dimensions and mass of all specimens were measured before and after the surface treatment. For these measurements a confocal microscope MarSurf CM Explorer, a digital micrometer BGS technic 8427 (resolution 0.001 mm), a digital electronic calliper (resolution 0.01mm) and a scale KERN 572 were used.

The efficiency of the surface treatment was evaluated by the means of the mass removal rate, *MRR*, which is calculated as given in Eq. (1)

$$MRR = \frac{\Delta m}{\tau} \qquad (1)$$

where Δm is the mass difference before and after polishing in (mg), τ is the process duration in (s).

The specimens were polished using PEP with applied direct voltage *U* at 300 V and / or 330 V. The electrolyte, which was water-based 0.3 M $(NH_4)_2SO_4$ solution, temperature was ca. t_{el} = 75 °C. The electrolyte temperature was selected based on the previous experience on PEP treating stainless steel parts.

Specimen 1 was polished in two-step bath-PEP process, i.e. it was immersed into the electrolyte bath, starting at *U* = 330 V. In the second step, it was polished using the same PEP mode at *U* = 300 V. All other specimens were polished at *U* = 300 V regardless of the PEP mode.

The goal of the surface treatment of the analyzed specimens was to achieve a smooth final surface with high mechanical integrity. Provided that the surface of as-built specimens has extremely poor quality, it was anticipated that the duration of PEP alone would be too time-intensive. Therefore, a step of particle blasting was introduced before PEP, so that the initial surface roughness of the as-built specimens would be somewhat reduced. The media for the PB process was irregularly shaped stainless-steel particles.

Specimen 2 and Specimen 3 were particle blasted before bath-PEP for τ = 300 s at each of the following machine settings in this order 9000 RPM, 7000 RPM and 4000 RPM. The remaining specimens were particle blasted at 9000 RPM for total time of τ = 2400 s. The process was divided in four stages of 600 s. After each stage, specimens were inspected under a microscope evaluating the surface evolution. The PB treatment was stopped after no changes were detected between two consecutive micrographs. These specimens were polished employing a standing-wave-PEP approach, where a specimen is suspended in air by a holder and an electrolyte jet is applied onto the surface from below.

The conditions of each surface treatment for each specimen are given in Table 1: . Note that in case of the bath-PEP approach, the process had to be continuously interrupted for cooling down the electrolyte to maintain the process efficiency, while the standing-wave-PEP process was carried out without interruption since the electrolyte temperature did not rise significantly. However, specimens 7, 8 and 9 were treated in multiple stages in order to post-process the whole circumference of their middle section. To achieve that, specimen 7 was rotated by 120° after each 600 s of standing-wave-PEP, while specimens 8 and 9 were rotated by 180° after half of the process time.

Table 1: Applied surface treatment parameters.

Specimen No.	Particle blasting		Plasma electrolytic polishing							
	RPM	Time, τ_{PB}, min	Total time, τ_{PEP}, min	Voltage, U, V	Average current, I, A	Average temperature, t_{el}, °C		pH value	Electric conductivity, κ, mS/cm	Number of steps
						Start	End			
1	-	-	30	330-340	6	75.0	81.3	2.2	140 @ 75 °C	30
	-	-	30	300	5	75.2	77.4	2.2	118 @ 77 °C	30
2	9000; 7000; 4000	5 each RPM	30	300	5	75.4	77.9	2.2 – 2.5	118 @ 77 °C	30
3	9000; 7000; 4000	5 each RPM	30	300	3	74.9	80.0	2.2 – 2.5	139 @ 75 °C	15
4	9000	40	15	300	0.7	75.0	76.0			1
5	9000	40	10	300	0.9	74.8	75.8		111 @ 75 °C	1
6	9000	40	30	300	0.9	75.8				1
7	9000	40	30	300	1.3	74.9	75.2		104 @ 75 °C	3
8	9000	40	30	300	1.8	75.0	75.0	2.2	105 @ 75 °C	2
9	9000	40	60	300	1.2	74.8	75.4			2

Topology optimisation

The gained insights on the material properties of high-alloy X2CrMnNi16-7-4.5 steel and achievable surface quality of a bottom bracket of a cargo bike manufactured using the PBF-EB/M technology were applied in topology optimization, which was carried out using the commercially available software Altair® with the solver OptiStruct® 2021.2 and a DUAL2 optimization algorithm. Fatigue life constraints were implemented in the optimization, as it is not possible to use them as an objective function directly [37,38]. As it was discussed above, surface quality plays an important role when it comes to the mechanical integrity of a part. Research efforts were made to include the surface roughness parameters in fatigue analysis models [39]. Thus, in this study, methods for adding the surface roughness parameters as described in [39] into the topology optimization model were explored. In this work, a minimal weight objective function was paired with a strain-based fatigue constraint. The material data of PBF-EB/M specimens in as-built condition that were manufactured out of the austenitic high-alloy X2CrMnNi16-7-4.5 powder and reported in [18] were used for the topology optimization problem. The assumption that surface and bulk material is homogeneous and isotropic was made to simplify the model.

Results and discussion

High-alloy austenitic X2CrMnNi16-7-4.5 steel

The chemical composition of the atomized and blend powder is provided in Table 2. According to the data obtained using the optical microscopy, the microstructure of powder with 3 wt.% Ni consists of austenite, martensite and ferrite, for the powder with 6 wt.% Ni – of martensite and austenite and for the powder with 9 wt.% Ni – of austenite only. From Figure 1 one can see that the particle size distribution of the atomised powder is rather homogenous and normally distributed.

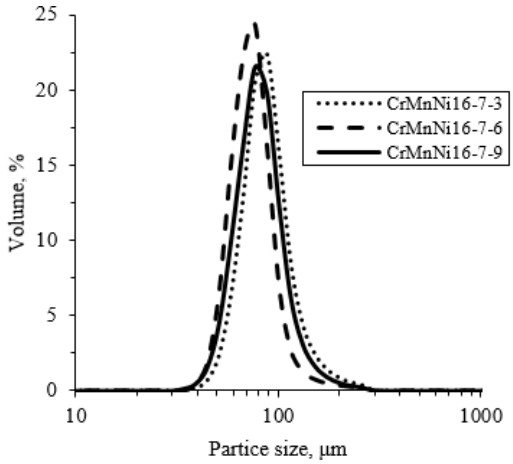

Figure 1: Particle size distribution of the atomised steel.

From Figure 2 it is clear, that powder particles are fairly spherical. However, particles of the powder with higher amount of nickel are more irregular in shape, although with less gas voids.

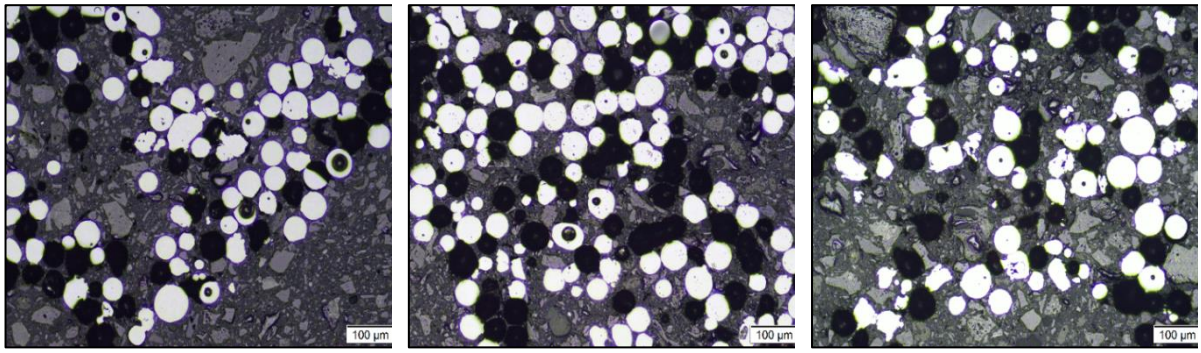

(a) (b) (c)

Figure 2: Micrographs of the atomised (a) 16-7-3, (b) 16-7-6 and (c) 16-7-9 steel powder after polishing.

Figure 3 shows that the particles in the obtained powder mix for PBF-EB/M process are mainly spherical with few so-called satellite particles attached to their surfaces. Nevertheless, these satellite particles did not negatively affect the powder flowability or otherwise impaired the building process.

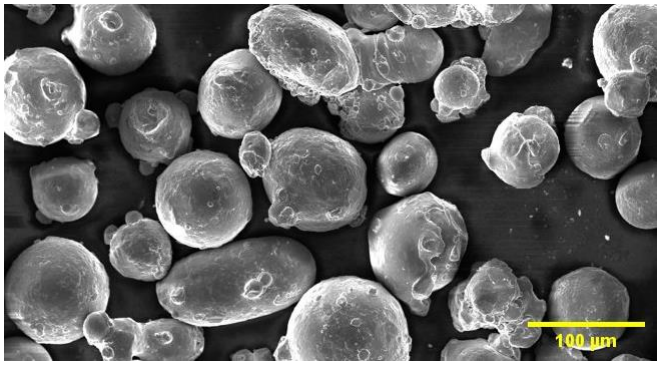

Figure 3: The morphology of the obtained powder mix X2CrMnNi16-7-4.5 obtained by SEM.

The PBF-EB/M F process parameters for manufacturing the investigated specimens are given in Table 3. The energy density applied on the specimen during the building process can be calculated as given in Eq. (2):

$$E_{vol} = \frac{P}{v\, h\, l} \qquad (2)$$

where, E_{vol} is volumetric energy density in (J mm^{-3}), P electron beam power in (W), v is scanning speed in (mm s^{-1}), h is hatch distance (mm), here h = 0.075 mm and l is the layer thickness in (mm), here l = 0.05 mm. The build temperature was kept constant at 900 °C. For hatching, a raster scan strategy with a 90° rotation in beam scan direction for each layer was used.

Table 2: Chemical composition of the produced powder.

X2CrMnNi 16-7-4.5	C, %	N, %	Si, %	Mn, %	Cr, %	Ni, %	Al, %	Nb, %	Ti, %	S, %	Mo, %
16-7-3	0.022	0.065	0.29	7.04	17.10	**3.23**	0.010	<0.01	<0.010	0.003	<0.01
16-7-6	0.021	0.079	0.11	6.87	16.20	**6.22**	0.007	<0.001	<0.001	0.003	0.003
16-7-9	0.020	0.073	1.04	6.99	15.70	**9.78**	0.030	0.020	<0.010	0.007	0.020
16-7-4.5	**0.020**	**0.066**	**0.44**	**7.03**	**16.82**	**4.54**	**0.014**	**0.012**	**0.01**	**0.0038**	**0.012**

Table 3: PBF-EB/M process parameters.

Specimen No.	Beam power, P, (W)	Scan speed, v, (mm s-1)
1 and 2	450	5000
3 und 4	450	2000
5	450	1500
6	450	1500
7, 8 and 9	450	2000

As shown in Figure 4 (a), the metallographic analysis of the as-built specimens reveals the defects like gas pores and surface notches that are ca. 600 µm deep. From the results of the crystallographic analysis, given in Figure 4 (b), one can see that the specimen demonstrates mainly face centred cubic (fcc) and body centred cubic (bcc) structure. Nevertheless, a high percentage of the bcc structure is attributed to specimen preparation induced martensitic transformation of metastable austenite. Finally, as it is seen Figure 4 (c) the specimen has a fine-grained structure, which shows a strong <101> texture in build direction.

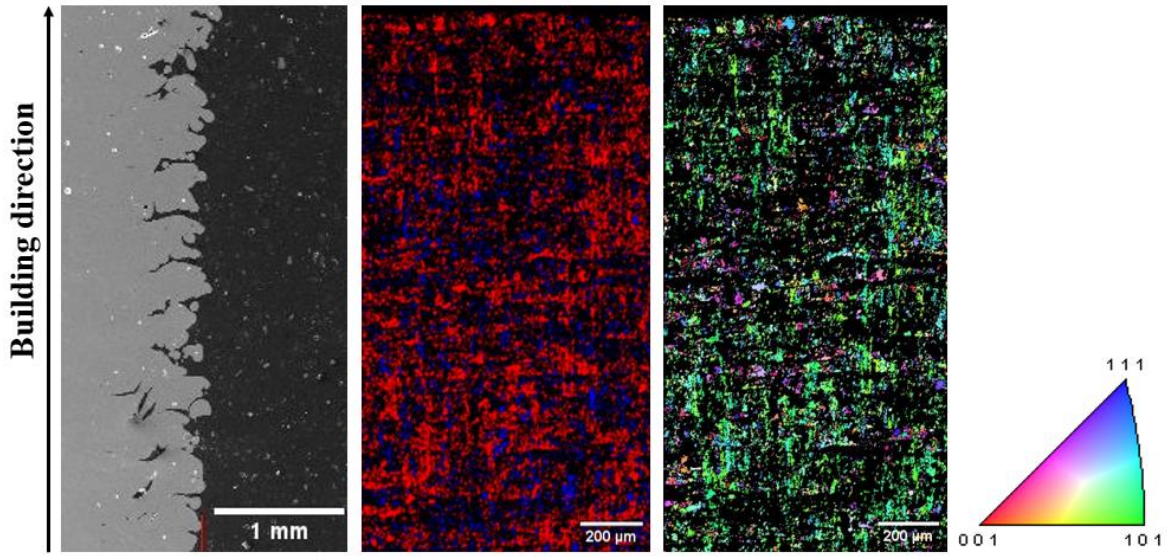

(a) (b) (c)

Figure 4: Cross-section of a specimen in as-built conditions manufactured with the same PBF-EB/M parameters as Specimen 1 (a), phase map of the as built specimen, where face centred cubic structure is shown in red and body centred cubic is shown in blue, and (c) orientation distribution of the specimen in the built direction.

In order to reduce the building defects, the optimisation of the PBF-EB/M process parameters took place by varying the parameter sets for the contouring step. For this purpose, changes were made to the focus offset, the scanning speed and the beam current. As one can see by comparing the cross-section of the specimens shown in Figure 4 (a) and Figure 5, the increase of the energy density on the specimen edges during the building process has a great positive impact on the resulting surface quality with the deepest surface notches being reduced from ca. 600 µm to ca. 250 µm. Unfortunately, gas pores inside the specimen were not avoided. These are a result of gas pores of the atomized powder which are not degassed during the building process.

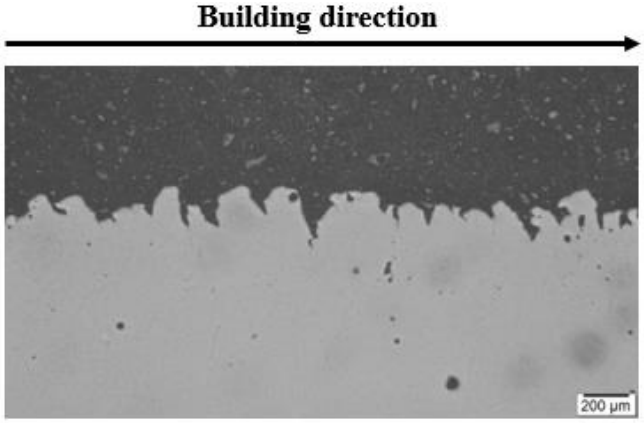

Figure 5: The cross-section of a specimen in as-built condition built using the same PBF-EB/M parameters as Specimen 3.

Surface treatment

In total 9 specimens were treated using a combination of a particle blasting, bath-PEP and standing-wave-PEP treatments. Figure 6 shows the representative specimens from each PBF-EB/M parameter group in as-built and after PEP conditions. Note that specimens from each group differ in shape and size. This is because the series of these specimens were designed for being used for different measurements and experiments that are not discussed in this article. It must be emphasised, though, that the shape and the size of a specimen, i.e. its total effective surface area has an impact only on the process current, I, and the rise in electrolyte temperature, t, during the process. Otherwise, the polishing results are not affected. Furthermore, variation in specimen geometry allows to gain insights on how they should be positioned during the process in order to achieve polishing objectives. The gained knowledge will be beneficial for polishing the bottom bracket of a cargo bike, described in section 0. In addition, a study on efficiency and impacts on the optical appearance of specimens after applying different modes of PEP is currently on going where specimens have been manufactured in a single build-job using the optimised PBF-EB/M parameters and are of the same shape.

By comparing photographs of the specimens in as-built conditions and after the surface treatment, it becomes obvious that the surface quality of the specimens is significantly improved in terms of gloss and surface roughness after the final PEP step. It also becomes apparent that a standing-wave-PEP provides comparable or even better polishing results in a shorter time.

By analysing the material removal rate, *MRR*, given in Figure 7, it is seen that bath-PEP, especially at U = 300 V, is more efficient as the *MRR* values are more than three times higher than those for the standing-wave-PEP. However, it is noticeable that specimens are fully, i.e. whole surface area, immersed into the electrolyte. Thus, the material is ablated all over the specimen. During the standing-wave-PEP processes, on the other hand, only a selected specimen area is exposed to the process, thus the material is removed only from a specific location on a specimen. It is also interesting to note that with increasing PEP time, *MRR* is not increasing accordingly, as it might be expected. On the contrary, with increasing τ_{PEP} *MRR* is getting lower. This is because PEP is self-focusing on the highest surface peaks, which are then ablated. With increasing τ_{PEP}, surface gets smoother, thus less surface peaks are to be removed, i.e., less material is ablated in the same time.

Furthermore, by comparing the thickness, σ, of the ablated material layer for each specimen, given in Figure 8, one can see that the standing-wave-PEP is able to ablate

almost twice the thickness in the same exposure time as bath-PEP. Once again, in the bath-PEP this layer is ablated from all sides of a specimen, while in standing-wave-PEP from only selected area. PB, on the other hand, even after τ = 2400 s of the process duration, could remove only δ = 0.12 mm of surface roughness. However, considering the depth of the surface notches of the as-built specimens discussed in paragraph 0, PB is of high importance as it can reduce the required PEP time significantly, especially when the bath-PEP approach is used.

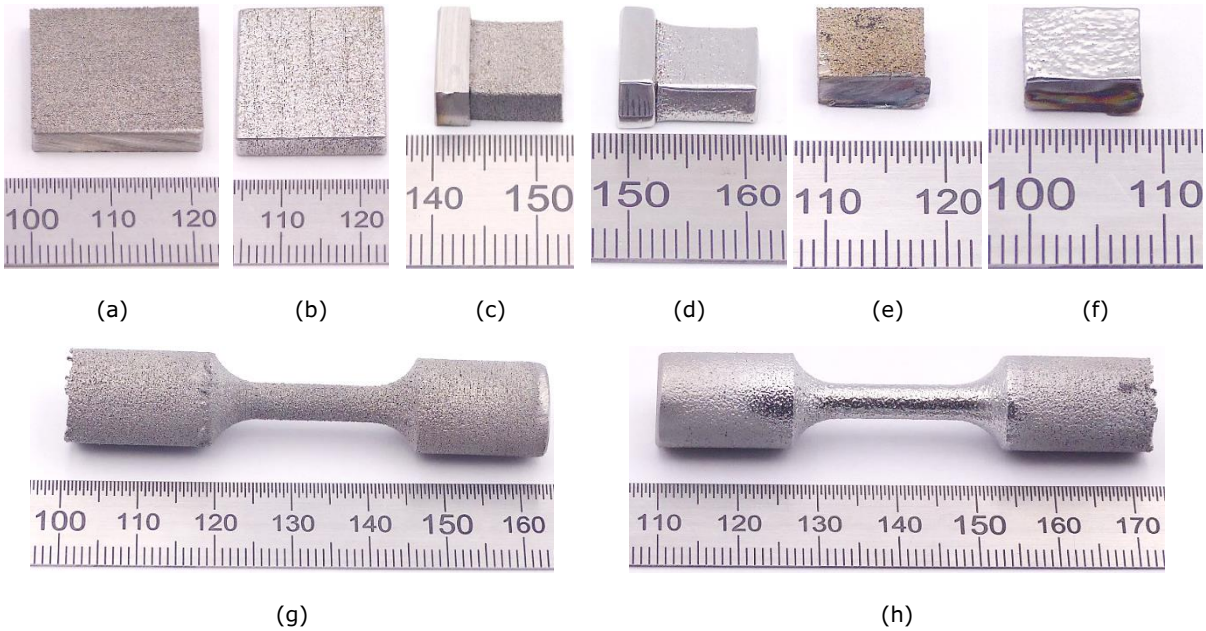

Figure 6: (a) Specimen 1 in as-built condition, (b) Specimen 1 after first stage of bath-PEP, (c) Specimen 3 in as-built condition (d) Specimen 3 after bath-PEP, (e) Specimen 4 in as-built condition, (f) Specimen 4 after standing-wave-PEP, (g) Specimen 7 in as-built condition and (h) Specimen 7 after standing-wave-PEP.

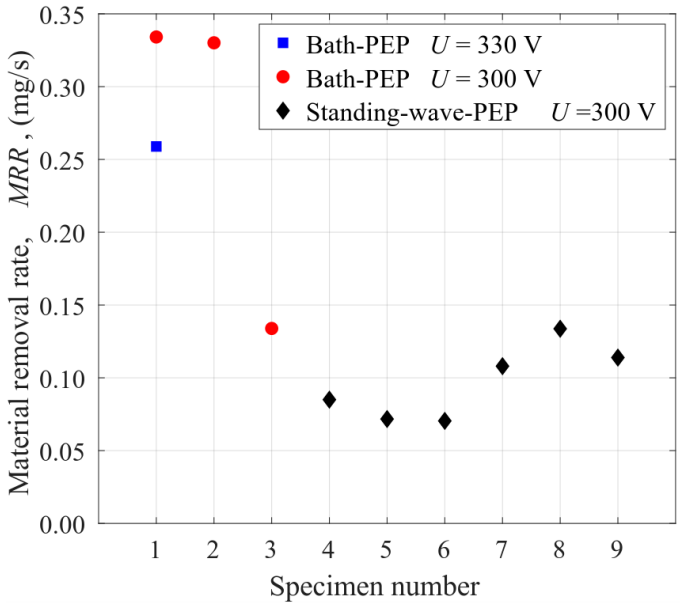

Figure 7: Material removal rate as a function of the PEP mode.

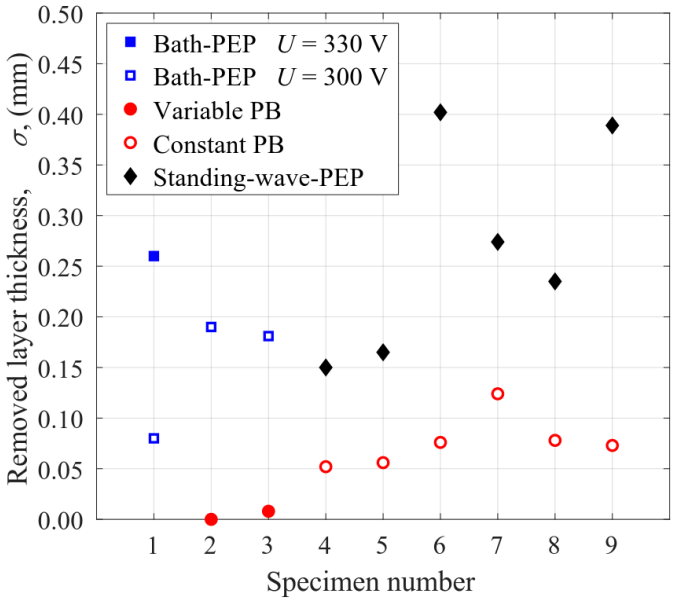

Figure 8: Thickness of the ablated material as a function of the surface treatment type.

Finally, a brief selection of the achieved surface smoothening is provided in Figure 9. It can be seen that the optimization of the PBF-EB/M process parameters leads to reduction of the depth and size of surface notches as well as their amount on the surface already in as-built condition. Furthermore, extreme peaks also could not be detected on the specimen built with optimized PBF-EB/M process parameters. The overall topology of the surface appears to be smoother and have less partly molten particles.

It can be seen that the surface quality after the respective surface treatment is significantly improved. Nevertheless, some defects still can be seen. Although, significantly less defects can be seen on the surface of a specimen with optimized PBF-EB/M process parameters. Provided that the depth of the surface notches of specimens built with not optimized PBF-EB/M parameters could be ca. 600 µm, and the total thickness of ablated material layer is ca. 190 µm, like for Specimen 2, it could be concluded that the apparent defects is the remaining surface roughness after the built process. The defects seen on Specimen 6 in Figure 9(d), provided the deepest surface notches being ca. 250 µm and the total thickness of the removed material ca. 478 µm, on the other hand, can be attributed to PBF-EB/M process defects, like gas pores.

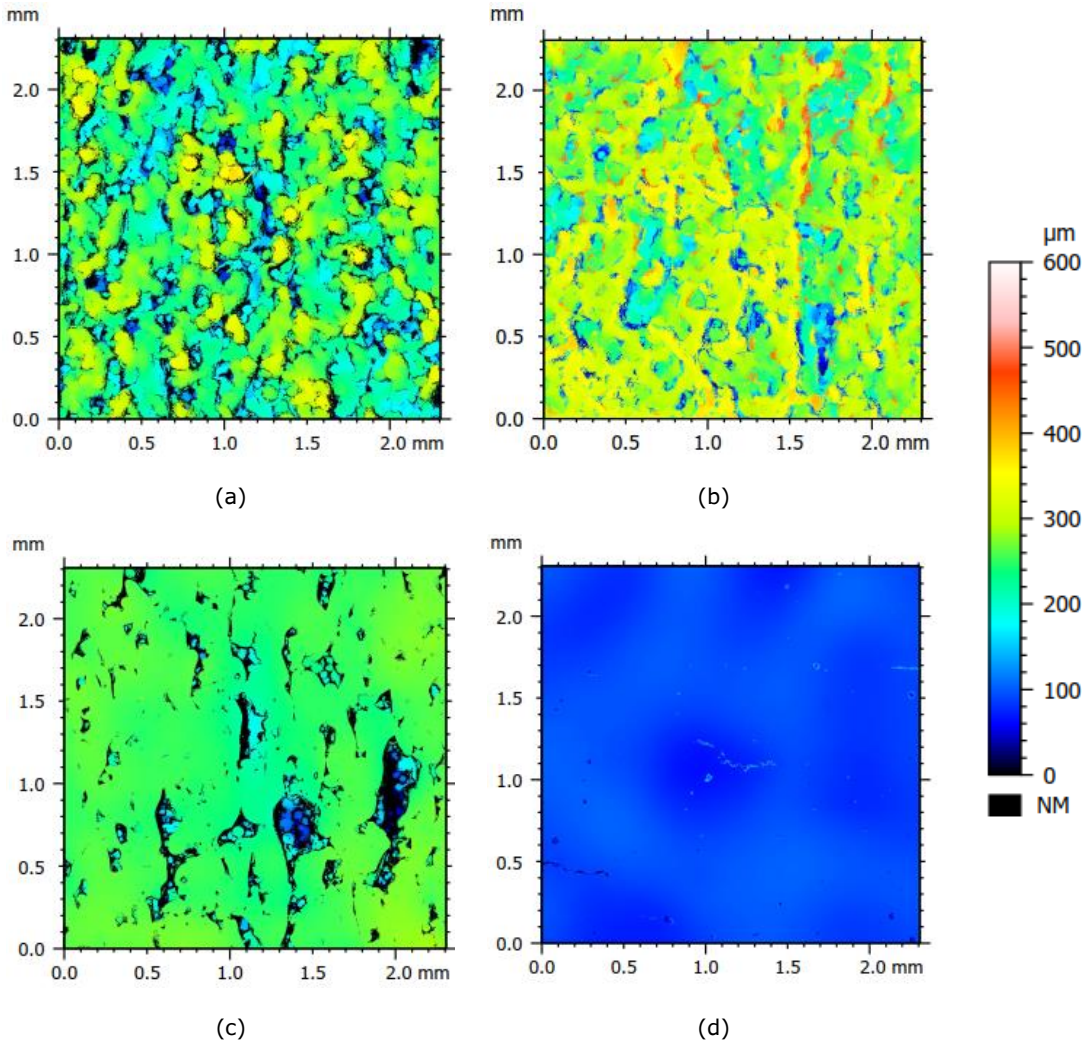

Figure 9: Surface topography of the selected specimens. (a) Specimen 2 in as-built condition, (b) Specimen 6 in as-built condition, (c) Specimen 2 after final bath-PEP step and (d) Specimen 6 after standing-wave-PEP.

Topology optimisation

As a case study, a bottom bracket of a cargo bike is topology optimized on the basis of the standard load cases for frames in DIN79010 [40]. The boundary conditions of the topology optimization model are given in Table 4. Additionally, minimum member size of 5 mm and a discreteness parameter are applied to improve the resulting design for additive manufacturing.

As this article only briefly presents the attempts to carry out the topology optimization of the part shown in Figure 10, the exact mathematical formulation of the topology optimization problem is omitted here and will be given in future articles related to the ongoing research.

Table 4: Boundary conditions of the topology optimisation model with the minimum weight objective function.

Volume fraction, χ, %	Life cycles, N, -	Displacement, Δl, (mm)		
		Pedal	Saddle	Front wheel
< 0.1	> 100,000	< 10.0	< 7.5	< 2.5

The results of a minimum weight objective function in Figure 10 show that the final structure is mainly governed by the displacement constraints. The influence of the limited lifetime constraint is only occurring in the thin rear-pointing structures. Consequently, the roughness-dependent modified material data do not influence the topology optimization result significantly. However, the subsequent fatigue analysis demonstrates that local surface quality improvements at critical part areas, i.e., stress concentration sites, have a substantial influence in the duration of the parts life, while the rest if the surface is of lower importance.

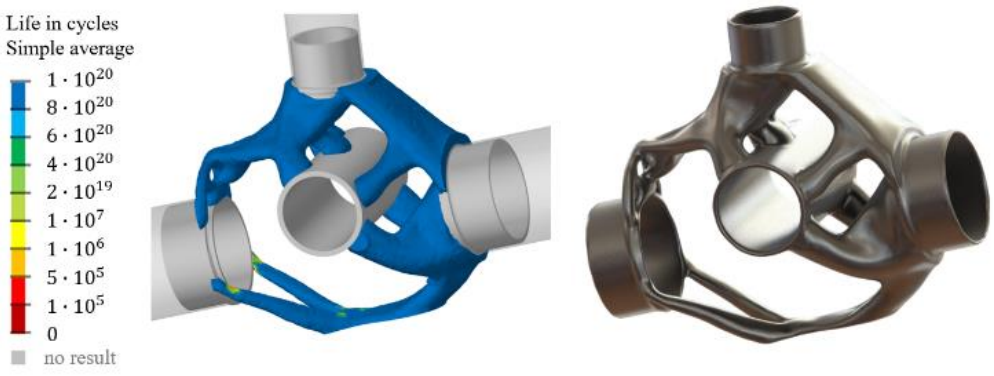

(a) (b)

Figure 10: Preliminary results of (a) the topology optimized geometry with life in cycles under pedalling and (b) the rendered view of the optimised structure.

Conclusion and outlook

In this study, preliminary results on processing a newly developed predominantly austenitic high-alloy X2CrMnNi16-7-4.5 steel using AM and PEP technologies are presented. The material was successfully manufactured using a layer based PBF-EB/M technology. Mechanical mixing of the powders led to an even distribution of the powder particles, which can be confirmed by the homogenous Ni content in the specimens. Furthermore, the alloy shows a fine-grained microstructure, which is important for developing parts with isotropic physical and mechanical properties.

The advanced surface treatment technologies like powder blasting and plasma electrolytic polishing also proved to be effective for refining the surface of additively manufactured austenitic high-alloy X2CrMnNi16-7-4.5 steel specimens. No selective material removal caused by a mismatch between the material chemical composition and the used electrolyte or material phase, i.e. martensite, austenite, ferrite, was observed. However, attempts to minimise the surface defects during the PBF-EB/M process should be made, since the duration of the post-processing processes for improving the surface integrity could increase to a matter of several hours. This would diminish the advantage of a rapid prototyping that AM technologies can offer. From all the tested surface refinement techniques, a combination of particle blasting with constant parameters and standing-wave-PEP proved to have the greatest efficiency. The later combination removed 60 % thicker material layer compared to the combination of variable PB and the bath-PEP. Finally, the standing-wave-PEP alone is able to remove more than twice as thick material layer as the bath-PEP in the same time.

Topology optimisation results of a bottom bracket of a cargo bike show that while surface quality of a part as a whole does not influence the duration of the such parts, surface quality on load concentration areas must be improved. For this purpose, a standing-wave-PEP is the most suitable technique, analysed in this article.

Acknowledgement

This measure is co-financed by tax funds on the basis of the budget approved by the Saxon state parliament. The project number is 100649753.

Contributions

Conceptualisation: K.N., S.L., A.S., J.K., A.W., M.W.; Methodology: K.N., K.N., M.P., S.L., A.S., J.K., A.W., M.W.; Software: K.N., J.K.; Validation: K.N., S.L., A.S., J.K., A.W., M.W.; Formal analysis: K.N., S.L., A.S., J.K.; Investigation: K.N., K.N., M.P., S.L., A.S., J.K.; Resources: K.N., K.N., M.P., S.L., A.S., J.K.; Data curation: K.N., K.N., M.P., S.L., A.S., J.K., A.W., M.W.; Writing-original draft: K.N.; Writing-review & editing: K.N., K.N., M.P., S.L., A.S., J.K., R.S., A.W., M.W., H.B., O.V., M.K., H.Z.; Visualisation: K.N.; Supervision & project administration: K.N., A.W., M.W., R.S., H.B., O.V., M.K., H.Z.; Funding acquisition: R.S., H.B., O.V., M.K., H.Z.

Literature

[1] A. Jahadakbar, M. Nematollahi, K. Safaei, P. Bayati, G. Giri, H. Dabbaghi, D. Dean, M. Elahinia, Design, Modeling, Additive Manufacturing, and Polishing of Stiffness-Modulated Porous Nitinol Bone Fixation Plates Followed by Thermomechanical and Composition Analysis, Metals (Basel). 10 (2020) 151. https://doi.org/10.3390/met10010151.

[2] H. Hou, E. Simsek, D. Stasak, N.A. Hasan, S. Qian, R. Ott, J. Cui, I. Takeuchi, Elastocaloric cooling of additive manufactured shape memory alloys with large latent heat, J. Phys. D. Appl. Phys. 50 (2017). https://doi.org/10.1088/1361-6463/aa85bf.

[3] K. Navickaitė, J. Liang, C.R.H. Bahl, S. Wieland, T. Buchenau, K. Engelbrecht, Experimental characterization of active magnetic regenerators constructed using laser beam melting technique, Appl. Therm. Eng. 174 (2020) 115297. https://doi.org/10.1016/j.applthermaleng.2020.115297.

[4] S. Wieland, J. Kagathara, E. Gärtner, V. Uhlenwinkel, M. Steinbacher, Powder, process parameters and heat treatment conditions for laser beam melting of LaFeSi-based alloys, in: Refrig. Sci. Technol., Darmstadt, 2018: pp. 27–32. https://doi.org/10.18462/iir.thermag.2018.0003.

[5] P. V. Trevizoli, R. Teyber, P.S. da Silveira, F. Scharf, S.M. Schillo, I. Niknia, P. Govindappa, T. V. Christiaanse, A. Rowe, Thermal-hydraulic evaluation of 3D printed microstructures, Appl. Therm. Eng. 160 (2019). https://doi.org/10.1016/j.applthermaleng.2019.113990.

[6] T. Lei, J. Alexandersen, B.S. Lazarov, F. Wang, J. Haertel, S. De Angelis, S. Sanna, O. Sigmund, K. Engelbrecht, Investment casting and experimental testing of heat sinks designed by topology optimization, Int. J. Heat Mass Transf. 127 (2018). https://doi.org/10.1016/j.ijheatmasstransfer.2018.07.060.

[7] K. Navickaitė, A. Mocerino, L. Cattani, F. Bozzoli, C. Bahl, K. Liltrop, X. Zhang, K. Engelbrecht, Enhanced heat transfer in tubes based on vascular heat exchangers in fish: Experimental investigation, Int. J. Heat Mass Transf. 137 (2019) 192–203. https://doi.org/10.1016/j.ijheatmasstransfer.2019.03.067.

[8] N. Shayesteh Moghaddam, S. Saedi, A. Amerinatanzi, A. Hinojos, A. Ramazani, J. Kundin, M.J. Mills, H. Karaca, M. Elahinia, Achieving superelasticity in additively manufactured NiTi in compression without post-process heat treatment, Sci. Rep. 9 (2019) 1–11. https://doi.org/10.1038/s41598-018-36641-4.

[9] D. Martínez-Maradiaga, O. V. Mishin, K. Engelbrecht, Thermal Properties of Selectively Laser-Melted AlSi10Mg Products with Different Densities, J. Mater. Eng. Perform. 29 (2020) 7125–7130. https://doi.org/10.1007/s11665-020-05192-z.

[10] L.E. Murr, E. Martinez, K.N. Amato, S.M. Gaytan, J. Hernandez, D.A. Ramirez, P.W. Shindo, F. Medina, R.B. Wicker, Fabrication of Metal and Alloy Components by Additive Manufacturing: Examples of 3D Materials Science, J. Mater. Res. Technol. 1 (2012) 42–54. https://doi.org/10.1016/S2238-7854(12)70009-1.

[11] B.T. Lejeune, R. Barua, E. Simsek, R.W. McCallum, R.T. Ott, M.J. Kramer, L.H. Lewis, Towards additive manufacturing of magnetocaloric working materials, Materialia 16 (2021) 101071. https://doi.org/10.1016/j.mtla.2021.101071.

[12] J.D. Avila, S. Bose, A. Bandyopadhyay, Additive manufacturing of titanium and titanium alloys for biomedical applications, Titan. Med. Dent. Appl. (2018) 325–343. https://doi.org/10.1016/B978-0-12-812456-7.00015-9.

[13] N.T. Aboulkhair, I. Maskery, I. Ashcroft, C.J. Tuck, The role of powder properties on the processability of Aluminium alloys in selective laser melting Lasers in Manufacturing Conference 2015 The role of powder properties on the processability

of Aluminium alloys in selective laser melting, Lasers Manuf. Conf. 2015 (2015).
[14] A. Vorontsov, S. Astafurov, E. Melnikov, V. Moskvina, E. Kolubaev, E. Astafurova, The microstructure, phase composition and tensile properties of austenitic stainless steel in a wire-feed electron beam melting combined with ultrasonic vibration, Mater. Sci. Eng. A 820 (2021) 141519. https://doi.org/10.1016/j.msea.2021.141519.
[15] E. Soares Barreto, M. Frey, J. Wegner, A. Jose, N. Neuber, R. Busch, S. Kleszczynski, L. Mädler, V. Uhlenwinkel, Properties of gas-atomized Cu-Ti-based metallic glass powders for additive manufacturing, Mater. Des. 215 (2022) 110519. https://doi.org/10.1016/j.matdes.2022.110519.
[16] M. Frey, J. Wegner, E.S. Barreto, L. Ruschel, N. Neuber, B. Adam, S.S. Riegler, H.-R. Jiang, G. Witt, N. Ellendt, V. Uhlenwinkel, S. Kleszczynski, R. Busch, Laser powder bed fusion of Cu-Ti-Zr-Ni bulk metallic glasses in the Vit101 alloy system, Addit. Manuf. 66 (2023) 103467. https://doi.org/10.1016/j.addma.2023.103467.
[17] A. Weidner, H. Biermann, Combination of Different In Situ Characterization Techniques and Scanning Electron Microscopy Investigations for a Comprehensive Description of the Tensile Deformation Behavior of a CrMnNi TRIP/TWIP Steel, JOM 67 (2015) 1729–1747. https://doi.org/10.1007/s11837-015-1456-y.
[18] H. Biermann, C.G. Aneziris, eds., Austenitic TRIP/TWIP Steels and Steel-Zirconia Composites, Springer International Publishing, Cham, 2020. https://doi.org/10.1007/978-3-030-42603-3.
[19] C. Schröder, A. Weiß, O. Volkova, Development of a new stainless austenitic CrMnNi steel using TRIP/TWIP effect for a high cold formability, Materwiss. Werksttech. 49 (2018) 577–590. https://doi.org/10.1002/mawe.201700278.
[20] J. Günther, F. Brenne, M. Droste, M. Wendler, O. Volkova, H. Biermann, T. Niendorf, Design of novel materials for additive manufacturing - Isotropic microstructure and high defect tolerance, Sci. Rep. 8 (2018) 1298. https://doi.org/10.1038/s41598-018-19376-0.
[21] A. Weidner, A. Glage, H. Biermann, In-situ characterization of the microstructure evolution during cyclic deformation of novel cast TRIP steel, Procedia Eng. 2 (2010) 1961–1971. https://doi.org/10.1016/j.proeng.2010.03.211.
[22] M. Wendler, A. Weiß, L. Krüger, J. Mola, A. Franke, A. Kovalev, S. Wolf, Effect of Manganese on Microstructure and Mechanical Properties of Cast High Alloyed CrMnNi-N Steels, Adv. Eng. Mater. 15 (2013) 558–565. https://doi.org/10.1002/adem.201200318.
[23] M. Wendler, M. Hauser, O. Fabrichnaya, L. Krüger, A. Weiß, J. Mola, Thermal and deformation-induced phase transformation behavior of Fe–15Cr–3Mn–3Ni–0.1N–(0.05–0.25)C austenitic and austenitic–martensitic cast stainless steels, Mater. Sci. Eng. A 645 (2015) 28–39. https://doi.org/10.1016/j.msea.2015.07.084.
[24] C. Quitzke, Q. Huang, H. Biermann, O. Volkova, M. Wendler, Influence of C and N on Strain-Induced Martensite Formation in Fe-15Cr-7Mn-4Ni-0.5Si Austenitic Steel, Materials (Basel). 14 (2021) 6502. https://doi.org/10.3390/ma14216502.
[25] S. Martin, C. Ullrich, D. Rafaja, Deformation of Austenitic CrMnNi TRIP/TWIP Steels: Nature and Role of the ε-martensite, Mater. Today Proc. 2 (2015) S643–S646. https://doi.org/10.1016/j.matpr.2015.07.366.
[26] T. Niendorf, F. Brenne, Steel showing twinning-induced plasticity processed by selective laser melting - An additively manufactured high performance material, Mater. Charact. 85 (2013) 57–63. https://doi.org/10.1016/j.matchar.2013.08.010.
[27] K. Engelbrecht, J. Tušek, S. Sanna, D. Eriksen, O. V. Mishin, C.R.H. Bahl, N. Pryds, Effects of surface finish and mechanical training on Ni-Ti sheets for elastocaloric

cooling, APL Mater. 4 (2016) 064110. https://doi.org/10.1063/1.4955131.
[28] T. DebRoy, H.L. Wei, J.S. Zuback, T. Mukherjee, J.W. Elmer, J.O. Milewski, A.M. Beese, A. Wilson-Heid, A. De, W. Zhang, Additive manufacturing of metallic components – Process, structure and properties, Prog. Mater. Sci. 92 (2018) 112–224. https://doi.org/10.1016/j.pmatsci.2017.10.001.
[29] K. Navickaitė, K. Nestler, F. Böttger-Hiller, C. Matias, A. Diskin, O. Golan, A. Garkun, E. Strokin, R. Biletskiy, D. Safranchik, H. Zeidler, Efficient polishing of additive manufactured titanium alloys, Procedia CIRP 108 (2022) 346–351. https://doi.org/10.1016/j.procir.2022.03.057.
[30] P.N. Belkin, S.A. Silkin, I.G. Dyakov, S. V. Burov, S.A. Kusmanov, Influence of Plasma Electrolytic Polishing Conditions on Surface Roughness of Steel, Elektron. Obrab. Mater. 55 (2019) 15–22. https://doi.org/10.5281/zenodo.3244425.
[31] K. Navickaitė, L. Ianniciello, J. Tušek, K. Engelbrecht, C.R.H. Bahl, M. Penzel, K. Nestler, F. Böttger-Hiller, H. Zeidler, Plasma Electrolytic Polishing of Nitinol: Investigation of Functional Properties, Materials (Basel). 14 (2021) 6450. https://doi.org/10.3390/ma14216450.
[32] L. Schorn, M. Wilkat, J. Lommen, M. Borelli, S. Muhammad, M. Rana, Plasma Electrolytic Polished Patient-Specific Orbital Implants in Clinical Use—A Technical Note, J. Pers. Med. 13 (2023). https://doi.org/10.3390/jpm13010148.
[33] V.N. Stepputat, H. Zeidler, D. Safranchik, E. Strokin, F. Böttger-Hiller, Investigation of Post-Processing of Additively Manufactured Nitinol Smart Springs with Plasma-Electrolytic Polishing, Materials (Basel). 14 (2021) 4093. https://doi.org/10.3390/ma14154093.
[34] A. Yerokhin, A. Pilkington, A. Matthews, Pulse current plasma assisted electrolytic cleaning of AISI 4340 steel, J. Mater. Process. Technol. 210 (2010) 54–63. https://doi.org/10.1016/j.jmatprotec.2009.08.018.
[35] A. Korolyov, A. Bubulis, J. Vėžys, Y. Aliakseyeu, V. Minchenya, V. Niss, D. Markin, Electrolytic plasma polishing of NiTi alloy, Math. Model. Eng. 7 (2021) 70–80. https://doi.org/10.21595/mme.2021.22351.
[36] K. Navickaitė, T. Böttger, K. Nestler, M. Penzel, S. Schröder, V. Stepputat, F. Böttger-Hiller, H. Zeidler, Electrolyte optimisation for effective plasma electrolytic polishing of brass, Results in Surfaces and Interfaces 12 (2023) 100133. https://doi.org/10.1016/j.rsurfi.2023.100133.
[37] E. Holmberg, B. Torstenfelt, A. Klarbring, Fatigue constrained topology optimization, Struct. Multidiscip. Optim. 50 (2014) 207–219. https://doi.org/10.1007/s00158-014-1054-6.
[38] J. Oest, E. Lund, Topology optimization with finite-life fatigue constraints, Struct. Multidiscip. Optim. 56 (2017) 1045–1059. https://doi.org/10.1007/s00158-017-1701-9.
[39] S. Lee, B. Rasoolian, D.F. Silva, J.W. Pegues, N. Shamsaei, Surface roughness parameter and modeling for fatigue behavior of additive manufactured parts: A non-destructive data-driven approach, Addit. Manuf. 46 (2021) 102094. https://doi.org/10.1016/j.addma.2021.102094.
[40] DIN 50100 Schwingfestigkeitsversuch-Durchführung und Auswertung von zyklischen Versuchen mit konstanter Lastamplitude für metallische Werkstoffproben und Bauteile, (2022). www.din.de.

Contacts

Kristina Navickaitė
Agricolastraße 1, 09959, Freiberg, Germany
E-Mail: kristina.navickaite@imkf.tu-freiberg.de
WEB: https://tu-freiberg.de/en/fakult4/imkf